EMMANUEL CARUYER

HABILITATION THESIS

IN PARTIAL FULFILMENT OF THE FRENCH HABILITATION
UNIVERSITÉ DE RENNES 1

NUMERICAL METHODS FOR WHITE MATTER MICROSTRUCTURE AND BRAIN STRUCTURAL CONNECTIVITY IN DIFFUSION MRI

COMMITTEE MEMBERS

Dr. Olivier Coulon, CNRS/Aix-Marseille University, FR – Reviewer.

Prof. Derek Jones, Cardiff University, UK – Reviewer.

Prof. Gloria Menegaz, University of Verona, IT – Reviewer.

Dr. Patrick Bouthemy, Inria center at Rennes University, FR – Examiner.

Prof. Tim Dyrby, DRCMR, DK – Examiner.

Prof. Pierre Maurel, University of Rennes 1, FR – Examiner.

Acknowledgements

I would like to express my gratitude to the reviewers and committee members who accepted to evaluate this work. I am also truly thankful to all the collaborators who contributed to this research, in particular to the students, trainees and postdoc who worked under my supervision. I would like to thank all my colleagues at Empenn and Neurinfo for for the great working environment they contribute to. Since this *habilitation* shall officially entitle me to supervise PhD students, I would like to thank the professors and researchers who have guided me in the past, in particular Ragini Verma and Rachid Deriche; your kind and enthusiastic mentoring will remain for me an endless source of inspiration. My thoughts go to Christian Barillot, who left us too early and will be acutely missing for my *habilitation* defence. Last I would like to thank Thanh and my family for their unfailing support along the years.

Contents

Introduction

This manuscript presents a review of our contributions to research in diffusion magnetic resonance imaging (MRI) methods over the past decade. It is organized in four chapters presenting original research, and a concluding chapter in which we discuss the perspectives.

In Chapter 1, we present mathematical methods we developed to represent and process the signal in **q**-space as well as **B**-tensor encoding. We show that proposing an adapted, continuous signal expansion is important since it may provide a compact representation useful for denoising, inverse problem solving and efficient sampling. In continuation, observing that commonly used metrics are derived from rotation-invariant features, we also proposed a mathematical framework to systematically characterize a family of such invariants.

In Chapter 2, we consider biophysical models, which are non-linear models relating tissue properties to the diffusion signal. The estimation of model parameters is in general ill-posed; however the accuracy of estimated parameters can be improved with a proper acquisition design. The use of generalized diffusion-encoding gradient waveforms have shown promising results in this context. The optimization of these waveforms is however tedious due to the possibly infinite dimension of the space of admissible gradient waveforms. We developed two family of methods, based on discrete sampling and sparse representation in the one hand, and on an optimization framework that increases the sensitivity to specific microstructure parameters compared to using the pulsed gradients as in the original Stejskal-Tanner sequence in the second hand.

In Chapter 3, we were interested in the reconstruction of brain structural connectivity using tractography. We believe validation is key to a larger endorsement by the community and its translation towards clinical applications. We have organized several competitions gathering international teams to exchange and compare their solutions to some of the many challenges raised by tractography and ultimately the reconstruction of a quantitative, microstructure-informed connectome. As a by-product of these competitions, we have released several open-source softwares and datasets to provide the community with easily accessible tools to validate their methods, using simulated data with a ground truth.

In Chapter 4 we present two clinical applications to which we contributed. The first application is related to diffusion MRI tractography in patients with brain tumour. We proposed estimation

method of the diffusion tensor to mitigate the effect of edema surrounding certain brain tumours. The second application concerns diffusion MRI of the spinal cord in patients with multiple sclerosis. We compared pre-processing methods for the correction of image distortions and evaluated the test-retest repeatability of quantitative diffusion MRI of the spine, an important feature for the longitudinal analysis of tissue changes induced by multiple sclerosis (MS).

Last, in Chapter 5, we present some perspectives and their associated challenges in the field of microstructure imaging and structural connectivity with MRI. The rapid uptake of machine learning in this area has provided successful practical response to some of these problems; this has also brought legitimate questions on the potential biases or inaccuracies that may be introduced by an inadequate model or training. We propose to contribute to this emerging field, building upon our expertise in simulation and mathematical representations in diffusion MRI. We will also develop rotation invariant reconstruction methods in microstructure, taking into account the full information in the spherical diffusion signal. Last, in order to fully benefit from the many degrees of freedom in gradient waveforms, we will propose a mathematical framework for the representation of this acquisition domain and facilitate acquisition design.

1
Adapted representation and sampling

The diffusion-weighted signal attenuation depends on the encoding gradient and is related to the diffusion properties of water molecules and the microscopic organization of biological tissues within which they diffuse. To exploit information in the signal, different families of mathematical models have been proposed, some of which aim at estimating general properties such as the ensemble average propagator or the diffusion tensor distribution. For these methods, we have shown that proposing an adapted, continuous signal expansion in **q**-space is important since it may provide a compact representation useful for denoising, inverse problem solving and efficient sampling (**Caruyer** and Deriche, 2012b; Merlet et al., 2011; **Caruyer** et al., 2013; Fick et al., 2016; Truffet et al., 2019). More recently, we have extended these **q**-space representations to the context of multidimensional diffusion encoding, to study the properties of the signal and give recommendations for sampling the space of axisymmetric **B**-tensors (Bates et al., 2020). Last, observing that commonly used metrics are derived from rotation-invariant features, we proposed a mathematical framework to systematically characterize a family of such features (**Caruyer** and Verma, 2015), which could be used as building blocks for elaborating new biomarkers.

1.1 Introduction

Digital signal processing emerged in the second half of the twentieth century and has found applications in audio, image or video processing to name a few. Each of these applications requires specific adaptations due to the mathematical domain on which the signal is defined. The main objectives of signal processing range from harmonic analysis, filtering to sampling and low dimension (sparse) representations. Similarly, in diffusion MRI different mathematical domains need to be considered, depending on the acquisition strategy and applications. High angular resolution diffusion imaging (HARDI) makes use of signal and fiber orientation distribution function representations on the sphere; the natural dual representation is spherical harmonics. In continuation, we have worked on natural representations for the signal in **q**-space and **B**-tensor encoding. We present in this chapter applications to signal regularization and optimal sampling. Last, we show how to take into account the geometry of the space by defining rotation-invariant features in HARDI.

1.2 *Adapted representations for q-space diffusion MRI*

The diffusion properties of water molecules within a voxel $\mathcal{V}$ can be summarized by the so-called ensemble average propagator (EAP)

$$P(\mathbf{r};\tau) = \int_{\mathcal{V}} p(\mathbf{r}+\mathbf{r_0};\mathbf{r_0},\tau)\mathrm{d}\mathbf{r_0},$$

which is the density of the average spin displacement over a time period τ.

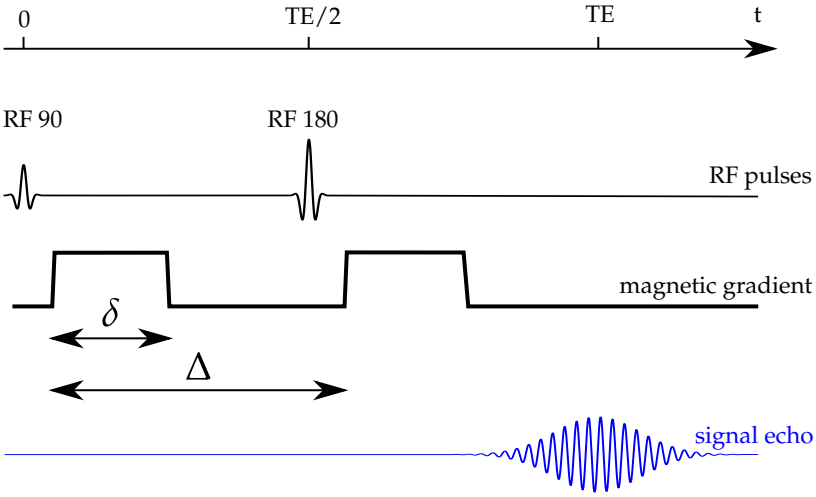

Figure 1.1: Simplified chronogram of a spin-echo magnetic resonance sequence, with a pair of pulsed magnetic gradients. δ is the pulse duration, while Δ denotes the pulse separation.

In a spin-echo MRI sequence, a pair of pulsed diffusion-encoding gradients can be added to measure diffusion (see Fig. 1.1). Under the short pulse assumption (Callaghan, 1993), the signal attenuation E is related to the propagator via a Fourier transform

$$E(\mathbf{q}) = \int P(\mathbf{r};\tau)\exp(-2i\pi\mathbf{q}\cdot\mathbf{r})\mathrm{d}\mathbf{r}, \tag{1.1}$$

where the diffusion time τ and the wavevector $\mathbf{q}$ are defined by

$$\tau = \Delta - \delta/3 \qquad \text{and} \qquad \mathbf{q} = \gamma\delta\mathbf{g}.$$

To exploit the link between the signal and the propagator, several strategies had been proposed – either based on the discrete Fourier transform and associated sampling of $E(\mathbf{q})$ on a regular grid (Wedeen et al., 2005), or by using intermediate continuous representations (Assemlal et al., 2009; Cheng et al., 2010; Descoteaux et al., 2011; Özarslan et al., 2013; Hosseinbor et al., 2013; **Caruyer** and Deriche, 2012a). We present in this section several contributions to the latter strategy and their impact on optimal acquisition design.

Laplacian-regularized MAP-MRI

Mean apparent propagator (MAP) MRI is a method based on the projection of the signal $E(\mathbf{q})$ onto an orthogonal basis of 3 dimensional, homogeneous Gauss-Hermite polynomials (Özarslan et al., 2013)

$$E_{\mathbf{a}}(q) = \sum_{N=0}^{N_{\max}} \sum_{(n_1,n_2,n_3)\in\mathcal{E}_N} a_{n_1n_2n_3}\psi_{n_1}(q_x;u_x)\psi_{n_2}(q_y;u_y)\psi_{n_3}(q_z;u_z),$$

where **a** is the vector of coefficients, u_j are scale factors and the set $\mathcal{E}_N = \{(n_1, n_2, n_3) \text{ s.t. } n_1 + n_2 + n_3 = N\}$. The Gauss-Hermite polynomial of degree n is defined as

$$\psi_n(q; u) = \frac{1}{\sqrt{2^{n+1}\pi n! u}} \exp\left(-\frac{q^2}{2u^2}\right) H_n(\frac{q}{u}). \tag{1.2}$$

The basis is adapted (orientation and scale) to the diffusion properties in each voxel, by first fitting a diffusion tensor model. The propagator, together with quantitative parameters such as the return to the origin probability (RTOP), return to the axis probability (RTAP) and return to the plane probability (RTPP), can be directly estimated from the coefficients **a**.

Observing that this approach is subject to noise and usually requires a large number of samples for an accurate estimation, we proposed to add a regularization constraint based on the norm of the Laplacian operator (Fick et al., 2016), a strategy that had been used successfully for other types of signal representations in diffusion MRI (Descoteaux et al., 2007; **Caruyer** and Deriche, 2012a). The regularized least squares estimation problem is

$$\tilde{\mathbf{a}} = \arg\min_{\mathbf{a}} \sum_{k=1}^{K} \left(E(\mathbf{q}_k) - E_{\mathbf{a}}(\mathbf{q}_k)\right)^2 + \lambda \int |\Delta E_{\mathbf{a}}(\mathbf{q})|^2 \mathrm{d}\mathbf{q}.$$

We show that the Laplacian has an analytical and compact expression in the coefficients in the basis, which incorporates seamlessly in the least squares estimation as a quadratic regularization term. In particular, this can be combined with the reconstruction under positivity constraint proposed in the original method (Özarslan et al., 2013).

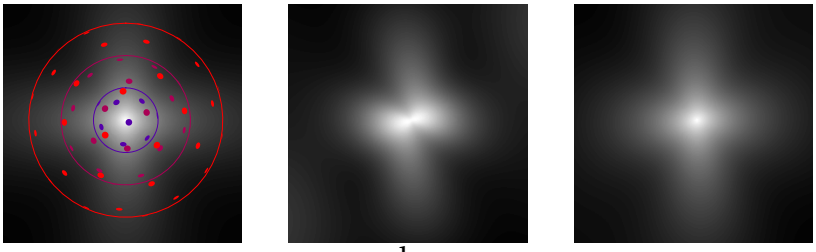

a b c

Figure 1.2: Example of a synthetic signal corrupted with Rician noise (SNR = 25) corresponding to a two-tensor model; the ground truth signal is represented (a) and the acquisition scheme, comprising 60 diffusion-weighted measurements over three shells ($b = 1000, 2000, 3000\ \mathrm{s\,mm^{-2}}$) is overlaid. We compare the reconstruction and interpolation with MAP-MRI without (b) and with (c) Laplace regularization.

The Laplacian-regularized solution is more robust to noise than the signal reconstructed taking into account the positivity constraint solely, as illustrated on Fig. 1.2. We also demonstrate that, beyond the EAP and derived scalar parameters (RTxP), reconstruction with MAPL can be used as a pre-processing step for denoising, interpolating and extrapolating the signal prior to biophysical model fitting. With this framework, we show that indices of axon diameter from the Axcaliber model (Assaf et al., 2008) and the orientation dispersion index from the NODDI model (Zhang et al., 2012) can both be estimated more accurately than fitting these models to the original data. MAPL is implemented in Dipy[1].

[1] DiPy, an open-source software library for medical image processing `https://dipy.org/`

1.3 *Multi-dimensional diffusion MRI*

In the previous section, we saw that the ensemble average propagator (EAP) can be reconstructed with q-space diffusion MRI. Note that since it is *ensemble* average, this description lacks to capture the full heterogeneity of diffusion properties in a voxel. To circumvent this, several approaches were proposed to model the micro-environments in a voxel with a diffusion tensor distribution, $f(\mathbf{D})$, that corresponds to a continuum of diffusive compartments – each of which is modeled with a diffusion tensor (Jian et al., 2007; Zhang et al., 2012; Scherrer et al., 2016). The average diffusion tensor, which is the first order moment of $f(\mathbf{D})$, is equivalent to the diffusion tensor defined classically. Higher order moments of the distribution give access to new and useful indices to characterize this heterogeneity.

Recently, it was shown that conventional diffusion encoding, using pulsed magnetic field gradients with constant orientations, are unable to reconstruct the full covariance of this distribution (Westin et al., 2016; Topgaard, 2017; Reymbaut et al., 2021). Q-space trajectory imaging, employing gradient waveforms $\mathbf{g}(t)$ with time-varying orientation, was proposed to access these parameters, from which we can define new indices such as the microscopic fractional anisotropy (μFA) or the orientation dispersion (OD). Within this framework, the signal attenuation is related to the diffusion tensor distribution through a Laplace transform

$$E(\mathbf{B}) = \int_{\mathcal{S}_n^+} f(\mathbf{D}) \exp(-\mathbf{B} : \mathbf{D}) \mathrm{d}\mathbf{D},$$

where the integral is defined on the space of positive semi-definite matrices $\mathcal{S}_n^+$. The matrix $\mathbf{B}$ above, generally referred to as the **B**-tensor, summarizes the acquisition parameters. It is defined from the gradient waveform $\mathbf{g}(t)$ by

$$\mathbf{B} = \int_0^{TE} \mathbf{q}(t)\mathbf{q}(t)^{\mathrm{T}} \mathrm{d}t, \qquad \text{where} \qquad \mathbf{q}(t) = \gamma \int_0^t \mathbf{g}(t')\mathrm{d}t'.$$

In the notations above, TE is the echo time and γ is the proton gyromagnetic ratio.

From a numerical perspective, contrarily to the Fourier transform, the inverse Laplace transform is an ill-posed problem (Topgaard, 2017). Similarly to what we contributed to develop in q-space, we proposed an orthogonal basis for representing the signal $E(\mathbf{B})$ (Bates et al., 2020). Observing that most methods proposed for white matter imaging employ encoding B-matrices with cylindrical geometry (Westin et al., 2016; Topgaard, 2017), we restricted the representation to the 4 dimensional space of symmetric positive matrices with cylindrical geometry, meaning that two of the three eigenvalues are equal. The basis we propose can be seen as an extension of the spherical polar Fourier basis (Assemlal et al., 2009):

$$E(\mathbf{B}) = \sum_{p=0}^{P} \sum_{n=0}^{N} \sum_{\ell=0}^{L} \sum_{m=-\ell}^{\ell} c_{pn\ell m} X_p(b_{||}) X_n(b_{\perp}) Y_\ell^m(\theta, \phi) \tag{1.3}$$

where $b_{||}$ and $b_{\perp}$ are the axial and radial eigenvalues of $\mathbf{B}$, respectively, and θ, ϕ are the polar and azimuthal angle defining the axis of symmetry of $\mathbf{B}$. The functions X_n are defined by

$$X_n(b) = \sqrt{\frac{n!}{\zeta^3(n+2)!}} \exp(-\frac{b}{2\zeta}) L_n^2(\frac{b}{\zeta})$$

where L_n^2 are the n-th generalized Laguerre polynomials of parameter 2, ζ is a scale factor, $Y_\ell^m(\theta, \phi)$ are the real spherical harmonics (SH) of maximum degree L (Descoteaux et al., 2007) and N is the maximum order. Using quadrature formulas, we also derive a *tight* sampling scheme for the truncated expansion (the minimal number of samples required is equal to the dimension of the basis) and an analytical reconstruction scheme. This provides an analytical, numerically stable estimation framework for the coefficients c_{pnlm} in Eq. 1.3.

Based on a dataset of Monte-Carlo simulated signals generated with Camino (Hall and Alexander, 2009), we observe that the truncated representation in this basis to low orders ($P = 6$ and $N = 3$ for $b_{||}$ and $b_{\perp}$, respectively) provide a close approximation and interpolation of the signal. We can also further observe that the angular bandwidth, L, can be adapted to $(b_{||}, b_{\perp})$: intuitively, the signal as a function of (θ, ϕ) has a sharper profile when the $\mathbf{B}$-tensor is either linear ($b_{||} \gg b_{\perp}$) or planar ($b_{||} \ll b_{\perp}$); the signal is otherwise smoother when $b = \mathrm{Tr}(\mathbf{B}) \to 0$ (see Fig. 1.3). This is an opportunity to further reduce the number of acquisitions, by adapting the number of directions to the angular resolution. In total, we show that a sampling scheme with a minimal number of samples $K = 280$ is sufficient for an accurate reconstruction of the signal in this basis, for $\mathbf{B}$-tensor eigenvalues up to $2000\,\mathrm{s\,mm^{-2}}$.

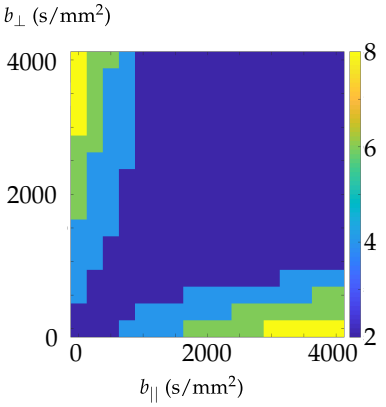

Figure 1.3: Angular band-limit of the signal (worst case across all microstructural substrates considered) represented versus the eigenvalues of the $\mathbf{B}$-tensor. The angular resolution can opportunely be tuned to the shape of the $\mathbf{B}$-tensor. Adapted from Bates et al. (2019).

1.4 *Rotation-invariant measures from diffusion data*

Equally important to the proper mathematical representation of the signal is the ability to extract meaningful information from this representation and construct imaging biomarkers. A first step towards this is the definition of rotation-invariant features; in diffusion tensor imaging, several such measures were developed, such as the fractional anisotropy (FA), the mean diffusivity (MD) and beyond (Westin et al., 2002; Ennis and Kindlmann, 2006). When it comes to characterize complex white matter with high angular resolution diffusion imaging (HARDI), the angular stucture is either represented using higher order tensors (Barmpoutis et al., 2012; Özarslan and Mareci, 2003) or spherical harmonics (Frank, 2002; Descoteaux et al., 2007). Some groups had proposed to extract rotation invariant measures from HARDI (Gur and Johnson, 2014; Schwab et al., 2013; Ghosh et al., 2012a,b), but there had been no systematic search for an independent set of invariants.

We introduced a method to derive all rotation-invariant features expressed as an order-t polynomial in the coefficients of the rank-L

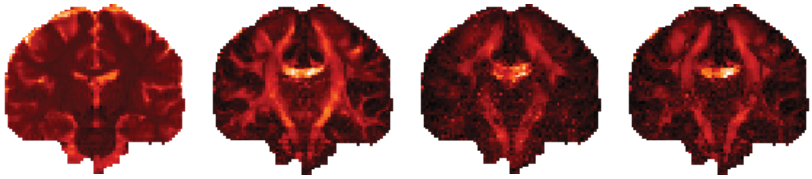

$L = 0, t = 1$ $L = 2, t = 2$ $L = 4, t = 3$ $L = 4, t = 3$

Figure 1.4: Rotation invariant polynomials of different degrees, t, computed from the SH coefficients at different ranks, L. Here, the SH coefficients represent the apparent diffusion coefficient (ADC) profile; note that the first invariant ($L = 0, t = 1$) is similar to the mean diffusivity. Adapted from **Caruyer** and Verma (2015).

spherical harmonics representation (**Caruyer** and Verma, 2015). We show that finding such polynomials is equivalent to solving a large system of equations; solutions were found numerically with an efficient implementation taking advantage of the sparse structure of the linear system of equations. From the set of solutions, using a pruning algorithm, we isolated a family of 12 (respectively 25) algebraically independant invariants for the spherical harmonics representation up to rank $L = 4$ (respectively $L = 6$). These invariant features show unique contrast in white matter (see Fig. 1.4). On a test-retest dataset, we showed that these new measures are reproducible across repetitions of the same subject, and exhibit subject-specific features. This set of invariants offers a new rotation-invariant representation of the HARDI signal, from which biomarkers could be constructed.

1.5 Conclusion

In this chapter, we have shown that understanding the structure of the signal is important, irrespective of the application. This has a positive impact on acquisition design, pre-processing and interpretation of the diffusion signal. The methods we derived are based on very general concepts (band-limitedness of the diffusion signal, regularity, rotation invariance). This prevents the rapid obsolescence of data acquired or processed using these concepts.

2
Microstructure-driven acquisition design

Biophysical modeling methods in diffusion MRI propose to relate the diffusion signal to microscopic tissue properties within the voxel. This family of methods therefore promise to provide very specific biomarkers and have been increasingly employed in clinical research for this reason. The estimation of model parameters is however in general ill-posed and the accuracy of estimated parameters can be improved with a proper acquisition design. The use of optimized diffusion-encoding gradient parameters and in particular generalized gradient waveforms have shown promising results in this context. This optimization is however tedious due to the possibly infinite dimension of the space of admissible gradient waveforms. In a first attempt to better characterize this space of gradient waveforms, we have proposed a dictionary learning and optimal sampling scheme, showing that we could successfully sub-sample the signal acquired for a set of gradient waveforms and yet recover the full signal as in the original dictionary (Truffet et al., 2019). For the specific problem of biophysical modeling, we have proposed in continuation an optimization framework (Truffet et al., 2020), showing that we can increase the sensitivity to specific microstructure parameters compared to using the pulsed gradients as in the original Stejskal-Tanner sequence. Being based on Monte-Carlo simulations, this framework is general and can be adapted to a large family of models and parameters of interest.

2.1 Introduction

When the diffusion is restricted, the expression of the spin-echo attenuation is relatively well known for simple confining geometries such as parallel planes, spheres or cylinders. While analytical formulas are known for pulsed gradients (Neuman, 1974; Callaghan, 1995), computing the response to generalized gradient encoding waveforms is done either via the matrix formalism (Callaghan, 1997) or the multiple correlation function approach (Grebenkov, 2007). For the hindered, extra-cellular space though, except in specific, periodic configurations (Moutal et al., 2020), the only method to predict the diffusion signal is usually via Monte-Carlo simulations (Hall and Alexander, 2009; Rafael-Patino et al., 2020). Besides, for arbitrary gradients, the acquisition domain is complex since the space of admissible gradient waveforms is virtually infinite dimensional. This makes the notion of *regularity* of the signal harder to capture than for parametric acquisition domains such as q-space or **B**-tensor encoding.

In this section, we first present a work that constructs a representation of the signal corresponding to non parametric gradient waveforms; this makes use of sparse transform and dictionary learning. Then, using Monte-Carlo simulations, we propose a framework to optimize gradient waveforms towards a higher Fisher information for specific microstructure parameters of interest.

2.2 *Sparse dictionary learning & optimal waveforms selection*

In this work, we proposed to start from a discrete set of K pseudo-random gradient waveforms (see Fig. 2.1) and evaluate the possibility to sub-sample the corresponding signal, while being able to predict the unseen data (Truffet et al., 2020). Using a set of example microstructure configurations modeling white matter fibers, that consist on parallel cylinders with random packing and gamma-distributed radii, we built a testing and training dataset of Monte-Carlo simulated signals using Camino (Hall and Alexander, 2009). The training dataset was used to learn a sparse representation (Mairal et al., 2010), $\mathbf{D}$, by optimizing

$$\arg\min_{\mathbf{x}_n,\mathbf{D}} \sum_{n=1}^{N} \left(\frac{1}{2} ||\mathbf{y}_n - \mathbf{D}\mathbf{x}_n||_2^2 + \lambda ||\mathbf{x}_n||_1 \right), \tag{2.1}$$

where $\mathbf{y}_n$ is the K-dimensional signal vector corresponding to the microstructure configuration n, $\mathbf{D}$ is the $K \times M$ learnt dictionary and $\mathbf{x}_n$ is the M-dimensional vector of coefficients, the sparsity of which is promoted with the ℓ_1 regularization penalty term in Eq. 2.1. The regularization weight was fixed to $\lambda = 0.15$ and the number of atoms (the size of the dictionary) was set to $M = 200$.

As a proof-of-concept, we propose to consider gradient waveforms $\mathbf{g}_k$ defined with a constant direction, $\mathbf{u}_k$, modulated by a pseudo-random piecewise constant function, taking values in $\{-g_{\max}, 0, g_{\max}\}$ (see Fig. 2.1). We generated 65 such temporal functions; combined with 40 directions uniformly spread on a sphere (Jones et al., 1999; **Caruyer** et al., 2013) this makes a total of $K = 2600$ gradient waveforms. We then find the best subset of measurements, $\Omega \subset \{1, \ldots, K\}$ minimizing the correlation between lines of the dictionary:

$$\arg\min_{\Omega} f(\Omega) = \sum_{k,l \in \Omega} \left(\sum_{m=1}^{M} \tilde{D}_{km} \tilde{D}_{lm} \right)^2,$$

where $\tilde{\mathbf{D}}$ is the dictionary $\mathbf{D}$ with its lines centered and reduced.

With this sub-sampling strategy, we show on our testing data that the coefficients $\mathbf{x}$ estimated with a fraction of the original measurements, $|\Omega| \ll K$, and the corresponding, extracted dictionary $\mathbf{D}_\Omega$, can be used to reconstruct the full signal with $\mathbf{y} = \mathbf{D}\mathbf{x}$ with high accuracy. The root mean squared error (RMSE) is about 0.005 for the signal reconstructed using a number of $|\Omega| = 30$ measurements. These results suggest that, despite the apparent complexity of the sampling domain and the diffusion-weighted attenuation, a sparse

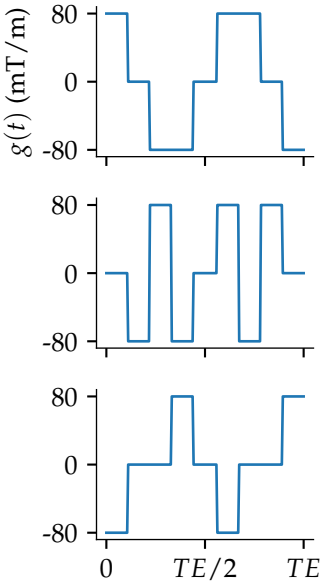

Figure 2.1: Example of the pseudo-random gradient waveforms used for the training and testing of sparse representation with dictionary learning. As a proof-of-concept, we propose to look at the signal response for piecewise constant gradient waveforms, taking values in the set $\{-g_{\max}, 0, g_{\max}\}$.

dictionary learning based representation can represent the regularity of the signal.

2.3 *Optimization of microstructure-sensitive waveforms*

Besides representing the signal, an important problem is that of optimizing gradient waveforms for the estimation of biophysical model parameters. In this work, we separated the orientation from the diffusion encoding by proposing a rotation-invariant method based on a genetic algorithm to maximize the sensitivity of the signal to specific microstructure features of interest (Truffet et al., 2020). We constructed microstructural substrates ready for Monte-Carlo simulation (Rafael-Patino et al., 2020) so that partial derivatives with respect to microstructure parameters, such as the mean axon radius or the intra-axonal volume fraction (IAVF), can be approximated using finite differences. From these derivatives, we can in turn compute the Fisher information associated to a specific acquisition protocol.

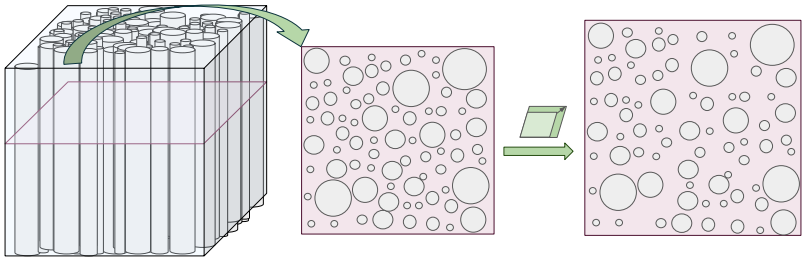

Figure 2.2: Example of a substrate that allows simulation of both intra-axonal and extra-axonal compartments. The procedure to study the local dependence (partial derivative) with respect to the IAVF is illustrated: the base configuration is transformed by scaling the voxel and the position of the cylinders, but without scaling the cylinder's radii. Adapted from Truffet et al. (2020)

Previous studies had targeted the same objective (Alexander, 2008; Drobnjak et al., 2010; Drobnjak and Alexander, 2011; Drobnjak et al., 2016); a major difference is that these prior studies were based on analytical models of the diffusion signal (Assaf and Basser, 2005; Assaf et al., 2008), where the diffusion in the extra-axonal compartment is approximated by an anisotropic Gaussian diffusion. In contrast, Monte-Carlo simulations offer greater flexibility on the definition of the substrate and a more realistic signal model (Rensonnet et al., 2019; Rafael-Patino et al., 2020).

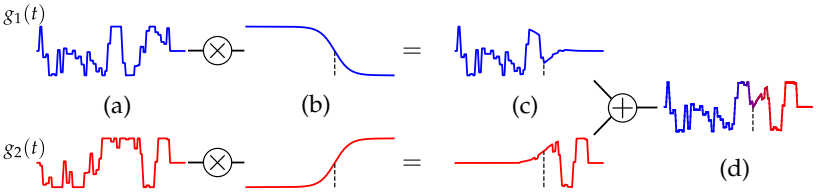

Figure 2.3: The cross-over is an important operation of the genetic algorithm; here we illustrate the result of the cross-over between two gradient waveforms, $g_1(t)$ and $g_2(t)$. NB: only the part of the waveform for $t \in [0, TE/2]$ is represented, the second part is simply defined by symmetry. Adapted from Truffet et al. (2020).

The objective was to optimize a set of diffusion encoding gradient waveforms, $\mathbf{g}(t) = g(t)\mathbf{u}$, defined in a constant direction, $\mathbf{u}$. The set of directions were chosen to spread the sphere uniformly (Jones et al., 1999), and the optimization was performed uniquely

on the gradient waveforms $g(t)$. Since the optimization domain is high dimensional, we anticipated a high probability of local minima; we therefore performed a stochastic optimization based on a genetic algorithm. Waveforms can be generated pseudo-randomly using a Markov chain (see for instance Fig. 2.3). For the genetic evolution of the algorithm, cross-overs (generation of a new waveform as a "mixture" of two parent waveforms) are defined as illustrated on Fig. 2.3.

Interestingly, the b-value associated to the waveforms provides a first approximation on the optimality of the waveform (see Fig. 2.4); but there also remains a large variability of Fisher information for a given b-value. We decided to limit the search in the b-value range $[1500, 3100]$ $\mathrm{s\,mm^{-2}}$. The genetic algorithm consisted in "generations" of 100 waveforms; the first generation contains only random waveforms, while starting from generation 2, most waveforms are obtained via cross-over of pairs of waveforms from the previous generation. After only 30 generations, we observe that the distribution of Fisher information stabilizes. The best candidate waveforms provide significantly higher Fisher information (around 1900) than the best PGSE acquisitions (around 1300).

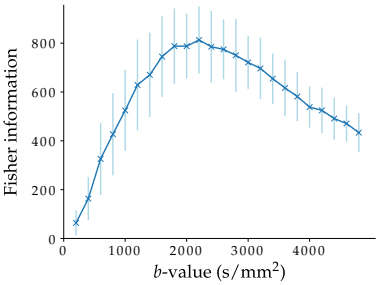

Figure 2.4: Fisher information as a function of the b-value; the bars correspond to the spread in Fisher information over 100 randomly generated waveforms for each b-value. Adapted from Truffet et al. (2020).

These results show that we can optimize waveforms and obtain, as a result, a better sensitivity to the IAVF than what was possible with PGSE. Since the waveforms are pseudo-randomly generated, interpreting the resulting optimized waveforms is somewhat complicated though; a local search optimization (gradient descent) would be interesting to further the optimization in this respect.

2.4 *Conclusion*

While representing the signal as a function of diffusion-encoding gradient waveforms or trajectories is complex, we have proposed a method using dictionary learning offering a compact representation of the signal. With this dictionary-based representation, we show that the signal acquired for a pseudo-random set of waveforms can be optimally sub-sampled, in such a way that unseen data can be predicted with good precision. In continuation, we have proposed a framework for the generation of diffusion encoding gradient waveforms optimized for the estimation of microstructure parameters of interest. The method is illustrated for the estimation of the IAVF in a model of white matter fibers; but since the framework makes use of Monte-Carlo simulations it can be generalized to a large family of substrates and microstructure parameters.

3
Validation of diffusion MRI-based tractography

We believe validation of tractography is key to a larger endorsement by the community and its translation towards clinical applications. We have organized several competitions gathering international teams to exchange and compare their solutions to some of the many challenges raised by tractography and ultimately the reconstruction of a quantitative, microstructure-informed connectome. As a by-product of these competitions, we have released several open-source softwares and datasets to provide the community with easily accessible tools to validate their methods, using simulated data with a ground truth.

3.1 Introduction

The reconstruction of major white matter fiber bundles using tractography was first proposed 30+ years ago (Mori et al., 1999); since then, the technique had a major impact on our knowledge of brain anatomy (Mori et al., 2005) and how it is affected by pathology. This method relies on the indirect relationship between the local, voxel-wise diffusion-weighted measurements and the axonal bundles pathways connecting distant grey matter regions. The reconstruction of these pathways is the result of a complex processing pipeline, the major steps of which are summarized in Fig. 3.1.

Due to the many steps involved in a tractography pipeline, there is a large variability in the reconstructed tractograms, which raises a question of reproducibility and reliability of the technique (Jones and Cercignani, 2010; Thomas et al., 2014; Maier-Hein et al., 2017; Rheault et al., 2020; Schilling et al., 2021). In this context, several validation methods have been proposed, either relying on physical phantoms (Fillard et al., 2011; Campbell et al., 2005; Guise et al., 2016), numerical models (Close et al., 2009; Neher et al., 2014; **Caruyer** et al., 2014), biological tracers (Delettre et al., 2019; Girard et al., 2020) or postmortem dissection (Zemmoura et al., 2014; Hau et al., 2017), see (Drobnjak et al., 2021) for a detailed review.

Over the last decade, we have contributed to this effort by organizing several competitions gathering international teams; we also released open-source software and datasets to provide the community with flexible validation methods and tools for the reconstruction of structural connectivity. This chapter proposes a tour of these contributions, putting them in perspective.

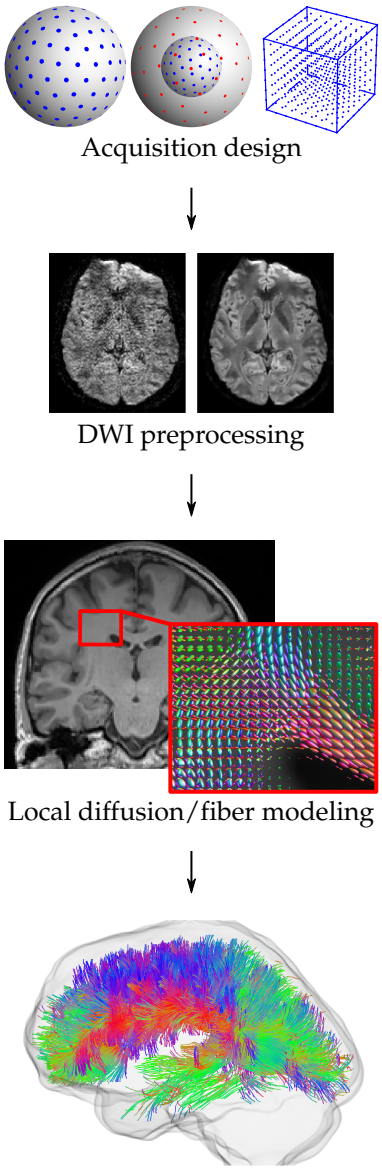

Figure 3.1: A typical diffusion MRI-based tractography pipeline; only the major steps are represented here. There is a large variability in tractography outcomes.

3.2 *Diffusion MRI reconstruction challenges*

Following the success of previous editions (MICCAI Fibercup challenge (2009) (Fillard et al., 2011), MICCAI DTI tractography challenge (2011 and 2012) (Pujol et al., 2015), IEEE ISBI Workshop on HARDI reconstruction (2012) (Daducci et al., 2014a)), we co-organized several diffusion reconstruction challenges[1,2,3] in a collaborative effort to evaluate tractography algorithms. A common objective of these challenges was to propose a collection of simulated datasets with a known ground truth. Concomitant to the shift of interest of the community and the progress made in simulation, the focus of these three editions evolved towards the evaluation of quantitative, microstructure-informed tractography. We summarize in this section the organization and conclusions of these three challenges.

[1] The HARDI reconstruction challenge (2013), `http://hardi.epfl.ch/static/events/2013_ISBI/`

[2] The ISMRM tractography challenge (2015) `http://tractometer.org/ismrm_2015_challenge/`

[3] The MICCAI diffusion-simulated connectivity (DiSCo) challenge (2021) `http://hardi.epfl.ch/static/events/2021_challenge`

The HARDI reconstruction challenge (ISBI 2013)

The objective of the 2013 HARDI reconstruction challenge was to evaluate the effects of the estimation accuracy of intra-voxel fiber configurations on the quality of subsequent connectivity analyses. We created a digital phantom of spherical shape comprising 27 fiber bundles, connecting 53 regions together (see Fig. 3.2). Participants requested diffusion-weighted data customized to their own acquisition scheme within a predefined budget, the diffusion weighted images were simulated using a multicompartment diffusion model (see Section 3.3 for a detailed description) and corrupted with Rician distributed noise.

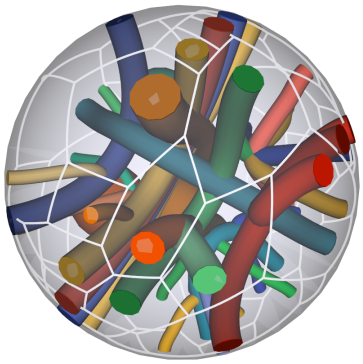

Figure 3.2: The 27 fiber bundles geometry of the ISBI 2013 HARDI reconstruction challenge and the "cortical" connected regions (outlined in white).

[4] The Tractometer – a tractography evaluation tool `http://tractometer.org/`

In total, the challenge received 17 submissions from 8 different groups; the task was to detect and estimate intra-voxel fiber orientations. We evaluated the impact on the quality of subsequent connectivity analyses using the Tractometer[4] (Côté et al., 2013). In a nutshell the strategy is to perfom tracking with standard algorithms in the literature, and compute statistics (average, best/worst case) on the computed tractograms, such as the number of valid/invalid bundles. We also computed two scores measuring the local accuracy of the fiber orientation estimates: the correct estimation of the number of estimated fiber compartments and their angular precision.

One of the main findings (Houde et al., 2014) of this edition is that we cannot predict the performance of tractography looking solely at the average score in local reconstruction. This suggests that more than an average performance in local fiber direction, deciphering local fiber orientation in key areas is critical for tractography. When comparing the different strategies of reconstruction, we also noticed that denoising had a positive impact on tractography. Another important conclusion of this challenge is that even using ground truth fiber orientation distributions (FOD) as an input, all tractography pipelines find a ratio of nearly 3 invalid bundles reconstructed per valid bundles.

The 2013 challenge was based on artificial fiber geometries. This

has provided a valuable feedback on the weaknesses of current tractography method, however the applicability of these findings to in vivo white matter tractography needed to be confirmed.

The ISMRM 2015 tractography challenge

To get an evaluation of tractography in a more realistic scenario, we proposed in the 2015 edition to simulate images starting from white matter fiber trajectories obtained with tractography in a real subject (Maier-Hein et al., 2017). After a full brain tractography of one of the HCP subject (Sotiropoulos et al., 2013), 25 fiber bundles were manually segmented by an anatomical expert (see Fig. 3.3), by defining inclusion and exclusion regions of interest (ROI). From these, T1- and diffusion-weighted images were simulated with Fiberfox (Neher et al., 2014).

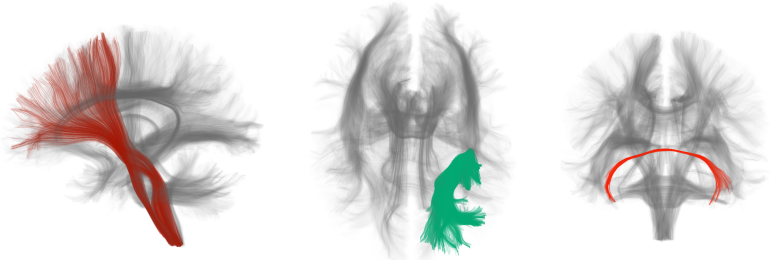

Figure 3.3: The ground truth fibers of the ISMRM 2015 tractography challenge, comprising projection, association and commisural fibers. A focus is shown on (from left to right) the left frontopontine tract (sagittal view), the left uncinate fasciculus (axial view) and the anterior commissure (coronal view).

This challenge gathered 20 team who submitted 96 tractography results in total. In line with the findings of the previous edition, the main outcome of the challenge was that most tractography methods were able to detect the 25 ground truth bundles, at the cost of a very large number of false positives. In trying to explain these false positives, we identified several regions where more than 3 fiber bundles were gathering – something which has later been referred to as the bottleneck effect (Schilling et al., 2022).

This challenge has exhibited several weaknesses in tractography as a detection problem. In the meantime, in a connectomics approach, there has been a growing interest in quantifying the connection *strength* between two regions, taking advantage of the microstructure information embedded in the MRI signal.

The 2021 DiSCo (diffusion-simulated connectivity) challenge

In order to evaluate quantitative connectivity reconstruction methods, we designed a collection of 3 phantoms (for training, validation and testing respectively) comprising in the order of 12 000 numerical tubular hollow fibers, with diameters ranging from 1.4 to 4.2 µm. From this model of microscopic fibers with macroscopic connections (each phantom fits in a 1 mm diameter sphere) connections (see Fig. 3.4, diffusion-weighted images of dimension $40 \times 40 \times 40$ were synthesized using Monte-Carlo simulation (Rafael-Patino et al., 2021).

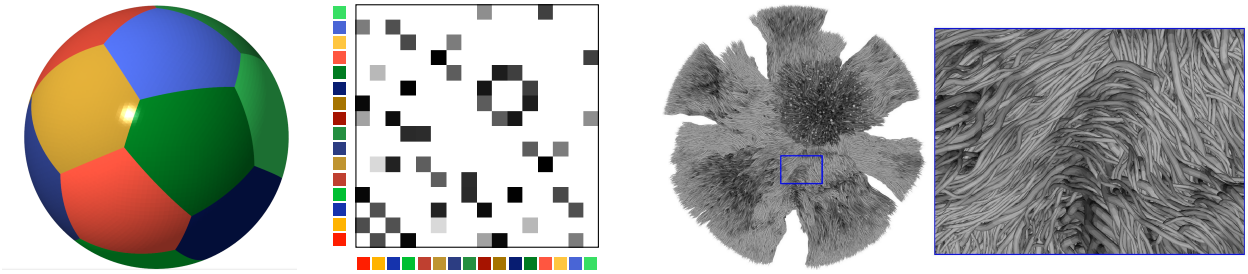

Figure 3.4: The ground truth "cortical" regions, connectivity matrix and fibers of the DiSCo challenge testing data.

3.3 *Phantomas: simulated diffusion MR phantom for the evaluation of structural connectivity pipelines*

For the needs of the ISBI 2013 challenge, we needed a flexible solution to create user-defined fiber geometries with some degree of control and simulate corresponding diffusion-weighted images. In contrast, existing solutions, such as the numerical fiber generator (NFG) (Close et al., 2009), had been designed to provide a fully automated solution to the creation of phantom geometries. After the challenge, we decided to make the code open-source: Phantomas (**Caruyer** et al., 2014) was first released in January 2014.

In Phantomas, a fiber bundle is defined as a tubular-shape object wrapped around its centerline; the trajectory of the centerline is fully specified by a set of control points using piecewise polynomials. A web application[5] was also implemented to help define fiber bundle trajectories with a graphical interface and mouse interaction. We also defined isotropic regions, to simulate contamination with cerebrospinal fluid (CSF) or free water, such as edematous regions that may surrounding brain tumor in patients (Parker et al., 2020).

[5] A web interface to help define fiber bundle trajectories `http://emmanuelcaruyer.com/phantomas-web/`

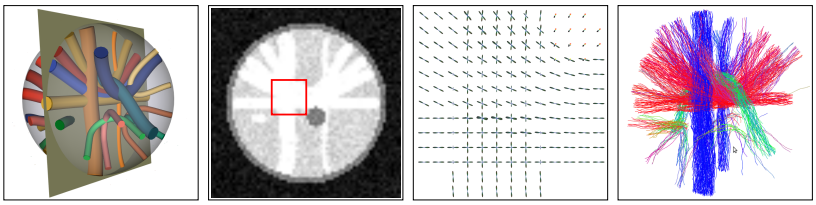

Figure 3.5: Digital phantom in diffusion MRI: fiber geometries (a), T1-weighted image (b), ground truth fiber orientation distribution (c), an example of fiber tracking result (d). Adapted from **Caruyer** et al. (2014).

From a collection of fiber trajectories and isotropic regions, T1- and T2-weighted images can be simulated, along with diffusion-weighted images. In every voxel, the diffusion is modeled by a distribution of Gaussian compartments. It is also possible to compute the ground truth fiber orientation distribution (FOD); a summary of these output is presented on Fig. 3.5.

3.4 *Conclusion*

We contributed to the field of validation of diffusion MRI tractography with the development of simulation methods to synthesize

diffusion-weighted images together with ground truth structural connectivity. The software and datasets derived from this work are open-source and have already been extensively used by the community. With DiSCo, the dataset that is created is unique since it combines macro-scale connectivity with the micro-scale complexity of interwoven axons. We believe this has contributed to expand our knowledge of current limits in tractography. In the future, we can expect this simulation field will also benefit from recent progress made possible by electron microscopy and synchrotron X-ray imaging.

4
Applications in clinical research

In the previous chapters, we have presented methods towards a better understanding of the measurement of diffusion in MRI and its validation in neuroimaging. In this chapter we present two clinical applications to which we contributed. The first application is related to diffusion MRI tractography in patients with brain tumour. We proposed estimation method of the diffusion tensor to mitigate the effect of edema surrounding certain brain tumours. The second application concerns diffusion MRI of the spinal cord in patients with multiple sclerosis. We compared pre-processing methods for the correction of image distortions and evaluated the test-retest repeatability of quantitative diffusion MRI of the spine, an important feature for the longitudinal analysis of tissue changes induced by multiple sclerosis (MS).

4.1 Free water elimination in peritumoral edema and improed tractography using clinical diffusion MRI

Characterization of healthy versus pathological tissue in the peritumoral area is confounded by the presence of edema, making free water estimation the key concern in modeling tissue microstructure (Pierpaoli and Jones, 2004; Pasternak et al., 2009). In these areas, we rely on a two-compartment model, for which the predicted signal is

$$E(b, \mathbf{u}; \mathbf{D}, f) = f \exp(-b\mathbf{u}^{\mathrm{T}}\mathbf{D}\mathbf{u}) + (1 - f) \exp(-bd),$$

where b is the diffusion weighting factor, $\mathbf{u}$ is the encoding gradient direction, $\mathbf{D}$ is the diffusion tensor modeling the tissue compartment and f is the tissue volume fraction.

One of the difficulties in fitting this model from clinical data is that estimating a two compartment model is an ill-posed problem if the acquisition consisted only in a single shell with a unique b-value (Pasternak et al., 2009; Scherrer and Warfield, 2010). This underscores the need for a robust free water elimination (FWE) method that estimates free water in pathological tissue but can be used with clinically prevalent single-shell diffusion tensor imaging data.

The solution to free water elimination (FWE) requires optimization, which relies on an initialization step. We proposed a novel initialization approach for FWE (Parker et al., 2020), called Free-water estimatoR using iNtErpolated iniTialization (FERNET), which improves the estimation of free water in edematous and infiltrated

peritumoral regions, using single-shell diffusion MRI data. The first strategy for the initialization of f, as found in the original paper (Pasternak et al., 2009), was solely based on the T_2-weighted information in the non diffusion-weighted ($b = 0$) image. We completed this with a second strategy, that uses the orientation average information in the diffusion-weighted signal and the prior information that the mean diffusivity in the white matter tissue compartment is expected around $0.6 \times 10^{-3}\,\mathrm{mm^2\,s^{-1}}$. The initialization which is proposed in FERNET is an interpolate between these two strategies.

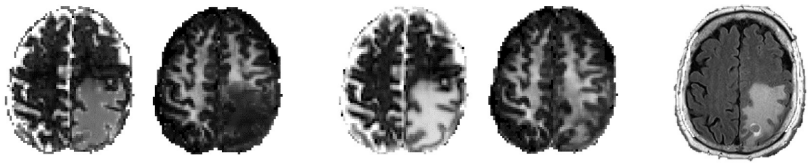

Figure 4.1: Comparison of the free water weight (FWW) and the FA of the tissue tensor obtained with the original initialization in (Pasternak et al., 2009) and FERNET in a patient with a metastatic brain tumor. The corrected FA map obtained with FERNET shows better agreement between the peritumoral region and the contralateral, healthy white matter compared to the original initialization. Adapted from Parker et al. (2020).

The method has been extensively investigated on data simulated with Phantomas (**Caruyer** et al., 2014) and healthy dataset. Additionally, it has been applied to clinically acquired data from brain tumor patients (see Fig. 4.1) to characterize the peritumoral region and improve tractography in it.

4.2 *Diffusion MRI within the cervical spinal cord in patients with multiple sclerosis*

Multiple sclerosis (MS) is a neuro-inflammatory disease and a major source of disability in young adults. The disease is associated with a range of clinical symptoms and progressive physical impairment. While brain imaging is now a standard diagnosis tool in clinical routine, there has been a recent interest in evaluating the extent of tissue damage in the spinal cord associated with the progression of symptoms in MS. Diffusion MRI using echo-planar imaging is challenging in the spinal cord; local changes in magnetic susceptibility due to the vicinity of air and bones cause strong field inhomogeneities, source of imaging artefacts.

Comparison of distortion correction methods

Post-processing methods were developed to reduce the impact of distortion, using a pair of images acquired with reverse phase encoding directions. However, these methods were mainly validated on brain images, more scarcely on spinal cord images. In this work (Snoussi et al., 2019, 2021), we compared the results of 3 distortion correction methods: HySCO (Ruthotto et al., 2012) as implemented in ACID/SPM Toolbox[1], Topup (Andersson et al., 2003) as implemented in FSL[2], Voss (Voss et al., 2006) (in-house implementation)

[1] ACID - Artefact correction in diffusion MRI – `http://www.diffusiontools.org/`

[2] FMRIB Software Library (FSL), `https://fsl.fmrib.ox.ac.uk/fsl/fslwiki`

and block-matching () as implemented in Anima[3]. The result of applying each of these methods on a sample subject is illustrated on Fig. 4.2.

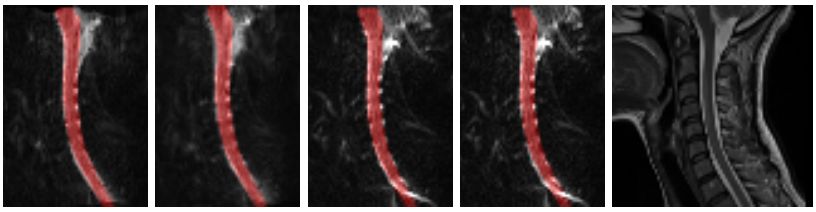

HySCO Topup Voss Uncorrected T_2-weighted

Figure 4.2: Result of different distortion correction methods applied to the same dataset. We overlay the spinal cord mask computed from the T_2-weighted image rigidly registered to the diffusion image.

[3] Anima, an open-source library for medical image processing https://github.com/Inria-Empenn/Anima-Public

We evaluated the performance of distortion correction algorithm with different, complementary metrics. Diffusion-weighted images (DWI) were acquired on a group of $N = 95$ subjects (29 controls and 66 MS patients); the protocol consists in thirty non-collinear DWI at $b = 900\ \mathrm{s\,mm^{-2}}$; six non-DWI measurements and one non-DWI with an opposite phase encoding direction were also acquired. The resolution is $2 \times 2 \times 2\ \mathrm{mm}^3$ and the acquisition is sagittal.

The first score measures the local alignment of the apparent centerline of the spine with the principal direction of diffusion. Anatomically, it is expected that the microscopic fiber direction is aligned with the macroscopic geometry of the spine. By expressing the principal axis of the diffusion in the local Frenet frame of the centerline, we can compute a concentration parameter (Mardia et al., 2000), which is a normalized measure in the range $[0, 1]$. The higher the concentration, the better the centerline of the spine is aligned with the diffusion direction. We also computed a cross-correlation score with the co-registered T_2-weighted image. Last, 3 experts were asked to rank the corrected images for each subject (blind assessment), presented along with the uncorrected image. HySCO and Voss perform best in terms of subjective evaluation, followed with BM and last Topup. All methods improve the realignment of the centerline of the spine with the diffusion direction; improvement is most significant with BM and Voss. Last, cross-correlation with the T_2-weighted image is improved ($p < 0.05$) with HySCO and BM. Based on these results, we would recommend HySCO for images acquired with a similar protocol.

Reproducibility of diffusion MRI scalar measures in spinal cord

One of the objectives of the EMISEP project[4] was to monitor the changes in spinal cord damage associated with the progression of motor deficit in MS. Reproducible measurements are the crux of longitudinal analyses; in this study (Snoussi et al., 2022) we investigated on a test-retest dataset the reproducibility of scalar measurements on regions of interests defined as intervertebral levels. Being based on a clinical dataset, we focused on the diffusion tensor and ball-and-stick models. For the former, we estimated the fractional anisotropy (FA),

[4] Early Spinal Cord Lesions and Late Disability in Relapsing Remitting Multiple Sclerosis Patients (EMISEP) project, `https://clinicaltrials.gov/ct2/show/NCT02117375`

axial, radial and mean diffusivities (AD, RD, MD); for the latter, we estimated the intrinsic diffusivity (ID), defined as the only positive eigenvalue of the stick, and the free water weight (FWW).

Intervertebral levels were segmented on the T_1-weighted image using the spinal cord toolbox[5] (De Leener et al., 2017) and the PAM50 template (De Leener et al., 2018); the labels were then co-registered to the diffusion images. The first observation is that there is a larger inter-subject variability in all metrics over vertebral levels at both ends of the imaging window when centered on the cervical spinal cord (C1-C2 and C6-C7); in continuation we decided to focus on the central part of the image (C3-C5). On the set of control subjects ($N = 8$), we computed the Bland-Altman plots and the 95% confidence interval, which enables to detect significant evolutions in patients between the baseline image (M0) and the follow-up scan (M12). Using these confidence intervals, we can therefore follow the longitudinal evolution of the same metrics for each patient, and identify abnormal trajectories associated with the pathology. Comparing metrics based on DTI and Ball-and-Stick suggests that both models provide complementary information. This suggests that even for clinical data, multi-compartment models provide novel information about the evolution of tissue microstructure, and should be included in the processing workflow.

[5] The spinal cord toolbox `https://spinalcordtoolbox.com/`

4.3 Conclusion

We have presented in this chapter two clinical applications of the methods we developed for diffusion MRI. The first method, which is related to multi-compartment modeling, has a direct application for brain tumors since it provides better free water elimination using clinical diffusion images. The maps generated and the subsequent tractography provide a valuable improvement in the context of pre-surgical planning. The second set of methods aim at improving diffusion MRI of the spinal cord, in terms of pre-processing and statistical analysis. In the context of MS, images of the cervical spinal cord offer complementary biomarkers, which may predict physical impairment better than when using brain lesions solely.

5
Perspectives

We have presented in this manuscript a summary of our research activity in the past decade. We have developed applied mathematical methods for the acquisition design, signal regularization, microstructure modeling and quantitative connectivity with diffusion MRI. We also translated some of these methods to clinical applications, mainly for brain tumors and spinal cord imaging in MS. Many challenges remain in the field of microstructure imaging and structural connectivity with MRI. The rapid uptake of machine learning in this area has provided successful practical response to some of these problems; this has also brought legitimate questions on the potential biases or inaccuracies that may be introduced by an inadequate model or training. We propose to contribute to this emerging field, building upon our expertise in simulation and mathematical representations in diffusion MRI. We will also develop rotation invariant reconstruction methods in microstructure, taking into account the full information in the spherical diffusion signal. Last, in order to fully benefit from the many degrees of freedom in gradient waveforms, we will propose a mathematical framework for the representation of this acquisition domain and facilitate acquisition design.

5.1 Introduction

As in many scientific domains, there has been a rapid rise of machine learning for estimating microstructure parameters, detect abnormalities related to pathology, or drive tractography. This can be partly explained by the improvement of simulation tools, which have become more realistic and more efficient. Yet, there is a pressing need to develop machine learning methods which are adapted to the constraints of diffusion MRI. One of these constraint is rotation invariance: we ambition to develop algorithms that leverage machine learning to identify a minimal set of rotation invariant features to estimate microstructure parameters of interest. In continuation, to take advantage of our expertise in simulation of large substrates that mimic brain connectivity (**Caruyer** et al., 2014; Rafael-Patino et al., 2021), we ambition to create a training dataset of such configurations and train a quantitative connectivity predictor using machine learning. Last, understanding the appropriate structure of the sampling domain is difficult for complex acquisitions that make use of **B**-tensor and gradient trajectories encoding. We will develop repre-

sentations of these sampling domains, taking into account their geometrical properties, defined by the invariance properties of diffusion measurement with MRI.

5.2 *Microstructure parameters and rotation invariants*

The diffusion tensor distribution (DTD) describes the intra-voxel diffusion as a continuum of isolated micro-environments, each of which characterized by a Gaussian diffusion. Although this method is not novel (Jian et al., 2007), the recent development of multi-dimensional diffusion encoding gave fresh impetus to the DTD (Topgaard, 2017; Westin et al., 2016) since the former provides unique access to specific properties such as the microscopic fractional anisotropy (μFA) or the orientation dispersion (OD). An estimation method commonly used, called the spherical mean technique or powder averaging (Kaden et al., 2016; Topgaard, 2017), consists in first computing the rotation-invariant spherical mean of the signal and use it to estimate these statistics of the DTD. The same method has also been applied to the estimation of microstructure parameters such as the intra-axonal volume fraction (Li et al., 2019) or the (Afzali et al., 2020; Andersson et al., 2022).

Provided that the original sampling scheme contains a sufficient number of directions, adapted to the angular band limit of the signal and that these directions form a spherical design (**Caruyer** and Deriche, 2012b), there is a guarantee that the spherical mean (or powder average) of the signal is invariant to rotations, which is a desirable property. However, this is arguably just one of the many invariants of a spherical signal (**Caruyer** and Verma, 2015); for this reason the spherical mean may not be a sufficient statistic for the estimation of the parameters of interest. As a result, this estimation technique may be suboptimal, in that it does not take advantage of all the relevant information contained in the acquired signal. We propose to systematically search for the existence of sufficient statistics for parameters of interest in the DTD and microstructure models, and consequently propose minimal acquisition requirements for the estimation of these parameters.

This will benefit to a better acquisition and modelling in white matter and gray matter. Among the applications, we plan to investigate imaging biomarkers of gray matter neurodegeneration in Alzheimer's disease.

5.3 *Towards a more quantitative tractography*

Tractography filtering methods such as SIFT (Smith et al., 2013), LiFE (Caiafa and Pestilli, 2017) or COMMIT (Daducci et al., 2014b) have significantly improved connectivity estimation by reducing the number of false-positive connexions typically found by tractography algorithms. Yet a number of confounding factors remain for tractography to be truly quantitative and we believe that machine learning is

an interesting lead towards improving structural connectivity.

The recent development of efficient simulation methods provides a unique tool for the generation of arbitrary complex, microscopically realistic configurations of fiber bundles and their associated simulated diffusion-weighted images (Rafael-Patino et al., 2021). We ambition to create a supervised training/testing dataset and use it to train a network in order to predict structural connectivity. Due to the computational cost of simulation, one of the challenges will be to robustly train a model with a limited number of examples. We will also try to propose a hybrid approach, in which only part of the tractography pipeline will be trained. We will need to find a standardized way to represent the inputs of the tractography filtering method, so that this can be abstracted in a large dataset of training examples.

5.4 Acquisition design and quantitative tractography

In voxel-wise analysis, we have shown in the previous chapters that acquisition design needs to be adapted to the reconstruction problem at hand, in particular for microstructure modelling. Recently, the use of **B**-tensor encoding was also shown to be useful in the estimation of the fiber orientation distribution (Rensonnet et al., 2021; Jeurissen and Szczepankiewicz, 2021). Similarly, downstream the processing pipeline, the quantification of structural connectivity is impacted by acquisition parameters; however to our knowledge few groups have systematically investigated sampling strategies optimized for connectivity estimation. One of the advantages of dictionary-based representation methods such as COMMIT (Daducci et al., 2014b) is the direct relationship between the diffusion signal and the fiber bundles in the tractogram. We will evaluate the impact of different acquisition protocols on the accuracy of the reconstructed connectome. Extending our preliminary work in Truffet et al. (2019), our search for an optimized solution will be driven by properties of the dictionary necessary for a stable reconstruction in the theory of sparse reconstruction.

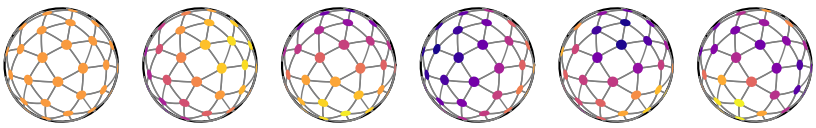

Figure 5.1: Example of the harmonic analysis on a discretely sampled sphere ($N = 60$ samples) represented as a graph; the 6 first eigenvectors of the graph Laplacian are illustrated. Adapted from an image courtesy of Constance Bocquillon.

For this optimization to be as exhaustive as possible, we will also work on efficient representation of gradient waveforms. The diffusion signal as a function of diffusion gradient encoding exhibit symmetries which need to be considered (shift invariance, antipodal symmetry). We will incorporate these in the definition of a metric in the space of gradient trajectories. Complementary to the discrete approach taken in Truffet et al. (2019), we propose to investigate signal processing on graphs (see illustration on Fig. 5.1) using the novel

metric we will define. We anticipate to lay the basis of an optimization of diffusion encoding towards a better estimation of the structural connectivity.

5.5 Conclusion

We conclude this manuscript with a research project, which aims at improving the clinical benefits of measuring water diffusion with MRI. Our project will focus on the development of new methods for quantitative tractography, both in terms of acquisition design and reconstruction. We will use data-driven approaches, combined with mathematical methods embedding the natural structure of the signal and the acquisition domain.

6
Bibliography

Maryam Afzali, Santiago Aja-Fernández, and Derek K Jones. Direction-averaged diffusion-weighted mri signal using different axisymmetric b-tensor encoding schemes. *Magnetic resonance in medicine*, 84(3):1579–1591, 2020.

Daniel C Alexander. A general framework for experiment design in diffusion mri and its application in measuring direct tissue-microstructure features. *Magnetic Resonance in Medicine: An Official Journal of the International Society for Magnetic Resonance in Medicine*, 60(2):439–448, 2008.

Jesper LR Andersson, Stefan Skare, and John Ashburner. How to correct susceptibility distortions in spin-echo echo-planar images: application to diffusion tensor imaging. *Neuroimage*, 20(2):870–888, 2003.

Mariam Andersson, Marco Pizzolato, Hans Martin Kjer, Katrine Forum Skodborg, Henrik Lundell, and Tim B Dyrby. Does powder averaging remove dispersion bias in diffusion mri diameter estimates within real 3d axonal architectures? *NeuroImage*, 248:118718, 2022.

Yaniv Assaf and Peter J Basser. Composite hindered and restricted model of diffusion (charmed) mr imaging of the human brain. *Neuroimage*, 27(1):48–58, 2005.

Yaniv Assaf, Tamar Blumenfeld-Katzir, Yossi Yovel, and Peter J Basser. AxCaliber: a method for measuring axon diameter distribution from diffusion MRI. *Magnetic Resonance in Medicine: An Official Journal of the International Society for Magnetic Resonance in Medicine*, 59(6):1347–1354, 2008.

Haz-Edine Assemlal, David Tschumperlé, and Luc Brun. Efficient and robust computation of pdf features from diffusion mr signal. *Medical image analysis*, 13(5):715–729, 2009.

Angelos Barmpoutis, Jeffrey Ho, and Baba C Vemuri. Approximating symmetric positive semidefinite tensors of even order. *SIAM journal on imaging sciences*, 5(1):434–464, 2012.

Alice Bates, Alessandro Daducci, and **Emmanuel Caruyer**. Multi-Dimensional Diffusion MRI Sampling Scheme: B-tensor Design and Accurate Signal Reconstruction. In *ISMRM 2019 - 27th Annual Meeting & Exhibition*, pages 1–4, Montréal, Canada, May 2019. URL https://www.hal.inserm.fr/inserm-02065830.

Alice Bates, Alessandro Daducci, Parastoo Sadeghi, and **Emmanuel Caruyer**. A 4D Basis and Sampling Scheme for the Tensor Encoded Multi-Dimensional Diffusion MRI Signal. *IEEE Signal Processing Letters*, 27:790–794, June 2020. DOI: 10.1109/LSP.2020.2991832. URL https://www.hal.inserm.fr/inserm-02881980.

Cesar F Caiafa and Franco Pestilli. Multidimensional encoding of brain connectomes. *Scientific reports*, 7(1):1–13, 2017.

Paul T Callaghan. *Principles of nuclear magnetic resonance microscopy*. Oxford University Press on Demand, 1993.

Paul T Callaghan. Pulsed-gradient spin-echo nmr for planar, cylindrical, and spherical pores under conditions of wall relaxation. *Journal of magnetic resonance, Series A*, 113(1):53–59, 1995.

Paul T Callaghan. A simple matrix formalism for spin echo analysis of restricted diffusion under generalized gradient waveforms. *Journal of Magnetic Resonance*, 129(1):74–84, 1997.

Jennifer SW Campbell, Kaleem Siddiqi, Vladimir V Rymar, Abbas F Sadikot, and G Bruce Pike. Flow-based fiber tracking with diffusion tensor and q-ball data: validation and comparison to principal diffusion direction techniques. *NeuroImage*, 27(4):725–736, 2005.

Emmanuel Caruyer and Rachid Deriche. Diffusion MRI Signal Reconstruction with Continuity Constraint and Optimal Regularization. *Medical Image Analysis*, 16(6):1113–1120, 2012a. DOI: 10.1016/j.media.2012.06.011. URL https://hal.inria.fr/hal-00711883.

Emmanuel Caruyer and Rachid Deriche. A Computational Framework for Experimental Design in Diffusion MRI. In *CDMRI - MICCAI Workshop on Computational Diffusion MRI*, Nice, France, October 2012b. URL https://hal.inria.fr/hal-00747700.

Emmanuel Caruyer and Ragini Verma. On facilitating the use of HARDI in population studies by creating rotation-invariant markers. *Medical Image Analysis*, 20(1):87–96, February 2015. DOI: 10.1016/j.media.2014.10.009. URL https://hal.archives-ouvertes.fr/hal-01090154.

Emmanuel Caruyer, Christophe Lenglet, Guillermo Sapiro, and Rachid Deriche. Design of multishell sampling schemes with uniform coverage in diffusion MRI. *Magnetic Resonance in Medicine*, 69(6):1534–1540, April 2013. DOI: 10.1002/mrm.24736. URL https://hal.inria.fr/hal-00821688.

Emmanuel Caruyer, Alessandro Daducci, Maxime Descoteaux, Jean-Christophe Houde, Jean-Philippe Thiran, and Ragini Verma. Phantomas: a flexible software library to simulate diffusion MR phantoms. In *ISMRM*, Milan, Italy, May 2014. URL `https://hal.inria.fr/hal-00944644`.

Jian Cheng, Aurobrata Ghosh, Tianzi Jiang, and Rachid Deriche. Model-free and analytical eap reconstruction via spherical polar fourier diffusion mri. In *International Conference on Medical Image Computing and Computer-Assisted Intervention*, pages 590–597. Springer, 2010.

Thomas G Close, Jacques-Donald Tournier, Fernando Calamante, Leigh A Johnston, Iven Mareels, and Alan Connelly. A software tool to generate simulated white matter structures for the assessment of fibre-tracking algorithms. *NeuroImage*, 47(4):1288–1300, 2009.

Marc-Alexandre Côté, Gabriel Girard, Arnaud Boré, Eleftherios Garyfallidis, Jean-Christophe Houde, and Maxime Descoteaux. Tractometer: towards validation of tractography pipelines. *Medical image analysis*, 17(7):844–857, 2013.

Alessandro Daducci, Erick Canales Rodgriguez, Maxime Descoteaux, Eleftherios Garyfallidis, Yaniv Gur, Ying Chia Lin, Merry Mani, Sylvain L. Merlet, Michael Paquette, Alonso Ramirez-Manzanares, Marco Reisert, Paulo Reis Rodrigues, Farshid Sepehrband, **Emmanuel Caruyer**, Jeiran Choupan, Rachid Deriche, Mathews Jacob, Gloria Menegaz, Vesna Prckovska, Mariano Rivera, Yves Wiaux, and Jean-Philippe Thiran. Quantitative comparison of reconstruction methods for intra-voxel fiber recovery from diffusion MRI. *IEEE Transactions on Medical Imaging*, (99): 384–399, February 2014a. DOI: 10.1109/TMI.2013.2285500. URL `https://hal.inria.fr/hal-00908289`.

Alessandro Daducci, Alessandro Dal Palù, Alia Lemkaddem, and Jean-Philippe Thiran. Commit: Convex optimization modeling for microstructure informed tractography. *IEEE transactions on medical imaging*, 34(1):246–257, 2014b.

Benjamin De Leener, Simon Lévy, Sara M Dupont, Vladimir S Fonov, Nikola Stikov, D Louis Collins, Virginie Callot, and Julien Cohen-Adad. SCT: Spinal cord toolbox, an open-source software for processing spinal cord mri data. *Neuroimage*, 145:24–43, 2017.

Benjamin De Leener, Vladimir S Fonov, D Louis Collins, Virginie Callot, Nikola Stikov, and Julien Cohen-Adad. Pam50: Unbiased multimodal template of the brainstem and spinal cord aligned with the icbm152 space. *Neuroimage*, 165:170–179, 2018.

Céline Delettre, Arnaud Messé, Leigh-Anne Dell, Ophélie Foubet, Katja Heuer, Benoit Larrat, Sebastien Meriaux, Jean-Francois Mangin, Isabel Reillo, Camino de Juan Romero, et al. Comparison be-

tween diffusion mri tractography and histological tract-tracing of cortico-cortical structural connectivity in the ferret brain. *Network Neuroscience*, 3(4):1038–1050, 2019.

Maxime Descoteaux, Elaine Angelino, Shaun Fitzgibbons, and Rachid Deriche. Regularized, fast, and robust analytical q-ball imaging. *Magnetic Resonance in Medicine: An Official Journal of the International Society for Magnetic Resonance in Medicine*, 58(3):497–510, 2007.

Maxime Descoteaux, Rachid Deriche, Denis Le Bihan, Jean-François Mangin, and Cyril Poupon. Multiple q-shell diffusion propagator imaging. *Medical image analysis*, 15(4):603–621, 2011.

Ivana Drobnjak and Daniel C Alexander. Optimising time-varying gradient orientation for microstructure sensitivity in diffusion-weighted mr. *Journal of Magnetic Resonance*, 212(2):344–354, 2011.

Ivana Drobnjak, Bernard Siow, and Daniel C Alexander. Optimizing gradient waveforms for microstructure sensitivity in diffusion-weighted MR. *Journal of Magnetic Resonance*, 206(1):41–51, 2010.

Ivana Drobnjak, Hui Zhang, Andrada Ianuş, Enrico Kaden, and Daniel C Alexander. PGSE, OGSE, and sensitivity to axon diameter in diffusion MRI: Insight from a simulation study. *Magnetic resonance in medicine*, 75(2):688–700, 2016.

Ivana Drobnjak, Peter Neher, Cyril Poupon, and Tabinda Sarwar. Physical and digital phantoms for validating tractography and assessing artifacts. *NeuroImage*, 245:118704, 2021.

Daniel B Ennis and Gordon Kindlmann. Orthogonal tensor invariants and the analysis of diffusion tensor magnetic resonance images. *Magnetic Resonance in Medicine: An Official Journal of the International Society for Magnetic Resonance in Medicine*, 55(1):136–146, 2006.

Rutger H.J. Fick, Demian Wassermann, **Emmanuel Caruyer**, and Rachid Deriche. MAPL: Tissue Microstructure Estimation Using Laplacian-Regularized MAP-MRI and its Application to HCP Data. *NeuroImage*, 134:365–385, July 2016. DOI: 10.1016/j.neuroimage.2016.03.046. URL `https://hal.inria.fr/hal-01291929`.

Pierre Fillard, Maxime Descoteaux, Alvina Goh, Sylvain Gouttard, Ben Jeurissen, James Malcolm, Alonso Ramirez-Manzanares, Marco Reisert, Ken Sakaie, Fatima Tensaouti, et al. Quantitative evaluation of 10 tractography algorithms on a realistic diffusion mr phantom. *Neuroimage*, 56(1):220–234, 2011.

Lawrence R Frank. Characterization of anisotropy in high angular resolution diffusion-weighted mri. *Magnetic Resonance in Medicine: An Official Journal of the International Society for Magnetic Resonance in Medicine*, 47(6):1083–1099, 2002.

Aurobrata Ghosh, Théo Papadopoulo, and Rachid Deriche. Biomarkers for hardi: 2nd & 4th order tensor invariants. In *2012 9th IEEE International Symposium on Biomedical Imaging (ISBI)*, pages 26–29. IEEE, 2012a.

Aurobrata Ghosh, Théodore Papadopoulo, and Rachid Deriche. Generalized invariants of a 4th order tensor: Building blocks for new biomarkers in dmri. In *Proceedings of the Computation Diffusion MRI Workshop at the MICCAI Conference*, 2012b.

Gabriel Girard, Roberto Caminiti, Alexandra Battaglia-Mayer, Etienne St-Onge, Karen S Ambrosen, Simon F Eskildsen, Kristine Krug, Tim B Dyrby, Maxime Descoteaux, Jean-Philippe Thiran, and Giorgio M Innocenti. On the cortical connectivity in the macaque brain: A comparison of diffusion tractography and histological tracing data. *Neuroimage*, 221:117201, 2020.

Denis S Grebenkov. Nmr survey of reflected brownian motion. *Reviews of Modern Physics*, 79(3):1077, 2007.

Catarina Guise, Margarida M Fernandes, Joao M Nobrega, Sudhir Pathak, Walter Schneider, and Raul Fangueiro. Hollow polypropylene yarns as a biomimetic brain phantom for the validation of high-definition fiber tractography imaging. *ACS applied materials & interfaces*, 8(44):29960–29967, 2016.

Yaniv Gur and Chris R Johnson. Generalized hardi invariants by method of tensor contraction. In *2014 IEEE 11th international symposium on biomedical imaging (ISBI)*, pages 718–721. IEEE, 2014.

Matt G Hall and Daniel C Alexander. Convergence and parameter choice for monte-carlo simulations of diffusion mri. *IEEE transactions on medical imaging*, 28(9):1354–1364, 2009.

Janice Hau, Silvio Sarubbo, Jean Christophe Houde, Francesco Corsini, Gabriel Girard, Charles Deledalle, Fabrice Crivello, Laure Zago, Emmanuel Mellet, Gaël Jobard, et al. Revisiting the human uncinate fasciculus, its subcomponents and asymmetries with stem-based tractography and microdissection validation. *Brain Structure and Function*, 222(4):1645–1662, 2017.

A Pasha Hosseinbor, Moo K Chung, Yu-Chien Wu, and Andrew L Alexander. Bessel fourier orientation reconstruction (BFOR): An analytical diffusion propagator reconstruction for hybrid diffusion imaging and computation of q-space indices. *NeuroImage*, 64:650–670, 2013.

Jean-Christophe Houde, **Emmanuel Caruyer**, Alessandro Daducci, and Maxime Descoteaux. How should tractography go forward? A Tractometer evaluation of local reconstruction and tracking. In *ISMRM*, page 6470, Milan, Italy, May 2014. URL `https://hal.archives-ouvertes.fr/hal-01033816`.

Ben Jeurissen and Filip Szczepankiewicz. Multi-tissue spherical deconvolution of tensor-valued diffusion mri. *Neuroimage*, 245: 118717, 2021.

Bing Jian, Baba C Vemuri, Evren Özarslan, Paul R Carney, and Thomas H Mareci. A novel tensor distribution model for the diffusion-weighted mr signal. *NeuroImage*, 37(1):164–176, 2007.

Derek K Jones and Mara Cercignani. Twenty-five pitfalls in the analysis of diffusion mri data. *NMR in Biomedicine*, 23(7):803–820, 2010.

Derek K Jones, Mark A Horsfield, and Andrew Simmons. Optimal strategies for measuring diffusion in anisotropic systems by magnetic resonance imaging. *Magnetic Resonance in Medicine: An Official Journal of the International Society for Magnetic Resonance in Medicine*, 42(3):515–525, 1999.

Enrico Kaden, Nathaniel D Kelm, Robert P Carson, Mark D Does, and Daniel C Alexander. Multi-compartment microscopic diffusion imaging. *NeuroImage*, 139:346–359, 2016.

Hua Li, Ho Ming Chow, Diane C Chugani, and Harry T Chugani. Linking spherical mean diffusion weighted signal with intra-axonal volume fraction. *Magnetic resonance imaging*, 57:75–82, 2019.

Klaus H Maier-Hein, Peter F. Neher, Christophe Houde, Marc-Alexandre Côté, Eleftherios Garyfallidis, Jidan Zhong, Maxime Chamberland, Fang-Chen Yeh, Ying-Chia Lin, Qing Ji, Wilburn E. Reddick, John O. Glass, David Qixiang Chen, Yuanjing Feng, Chengfeng Gao, Ye Wu, Jieyan Ma, H. Renjie, Qiang Li, Carl-Fredrik Westin, Samuel Deslauriers-Gauthier, J. Omar Ocegueda González, Michael Paquette, Samuel St-Jean, Gabriel Girard, François Rheault, Jasmeen Sidhu, Chantal M. W. Tax, Fenghua Guo, Hamed Y. Mesri, Szabolcs Dávid, Martijn Froeling, Anneriet M. Heemskerk, Alexander Leemans, Arnaud Boré, Basile Pinsard, Christophe Bedetti, Matthieu Desrosiers, Bram Brambati, Julien Doyon, Alessia Sarica, Roberta Vasta, Antonio Cerasa, Aldo Quattrone, Jason Yeatman, Ali R. Khan, Wes Hodges, Simon Alexander, David Romascano, Muhamed Barakovic, Anna Auría, Oscar Esteban, Alia Lemkaddem, Jean-Philippe Thiran, H. Ertan Cetingul, Benjamin L. Odry, Boris Mailhé, Mariappan S. Nadar, Fabrizio M Pizzagalli, Gautam Prasad, Julio E. Villalon-Reina, Justin Galvis, Paul M. Thompson, Francisco de Santiago Requejo, Pedro Luque Laguna, Luis Miguel Lacerda, Rachel Barrett, Flavio Dell'acqua, Marco Catani, Laurent Petit, **Emmanuel Caruyer**, Alessandro Daducci, Tim Dyrby, Tim Holland-Letz, Claus C. Hilgetag, Bram Stieltjes, and Maxime Descoteaux. The challenge of mapping the human connectome based on diffusion tractography. *Nature Communications*, 8(1), December 2017. DOI: 10.1038/s41467-017-01285-x. URL `https://hal.inria.fr/hal-01631578`.

Julien Mairal, Francis Bach, Jean Ponce, and Guillermo Sapiro. Online learning for matrix factorization and sparse coding. *Journal of Machine Learning Research*, 11(1), 2010.

Kanti V Mardia, Peter E Jupp, and KV Mardia. *Directional statistics*, volume 2. Wiley Online Library, 2000.

Sylvain Merlet, **Emmanuel Caruyer**, and Rachid Deriche. Impact of radial and angular sampling on multiple shells acquisition in diffusion MRI. In Fichtinger, Gabor, Martel, Anne, Peters, and Terry, editors, *MICCAI 2011*, volume 6891 of *Lecture Notes in Computer Science*, pages 113–121, Toronto, Canada, September 2011. Springer. URL `https://hal.archives-ouvertes.fr/hal-00614387`.

Susumu Mori, Barbara J Crain, Vadappuram P Chacko, and Peter CM Van Zijl. Three-dimensional tracking of axonal projections in the brain by magnetic resonance imaging. *Annals of Neurology*, 45(2):265–269, 1999.

Susumu Mori, Setsu Wakana, Peter CM Van Zijl, and LM Nagae-Poetscher. *MRI atlas of human white matter*. Elsevier, 2005.

Nicolas Moutal, Antoine Moutal, and Denis Grebenkov. Diffusion nmr in periodic media: efficient computation and spectral properties. *Journal of Physics A: Mathematical and Theoretical*, 53(32):325201, 2020.

Peter F Neher, Frederik B Laun, Bram Stieltjes, and Klaus H Maier-Hein. Fiberfox: facilitating the creation of realistic white matter software phantoms. *Magnetic resonance in medicine*, 72(5):1460–1470, 2014.

CH Neuman. Spin echo of spins diffusing in a bounded medium. *The Journal of Chemical Physics*, 60(11):4508–4511, 1974.

Evren Özarslan and Thomas H Mareci. Generalized diffusion tensor imaging and analytical relationships between diffusion tensor imaging and high angular resolution diffusion imaging. *Magnetic Resonance in Medicine: An Official Journal of the International Society for Magnetic Resonance in Medicine*, 50(5):955–965, 2003.

Evren Özarslan, Cheng Guan Koay, Timothy M Shepherd, Michal E Komlosh, M Okan İrfanoğlu, Carlo Pierpaoli, and Peter J Basser. Mean apparent propagator (map) mri: a novel diffusion imaging method for mapping tissue microstructure. *NeuroImage*, 78:16–32, 2013.

Drew Parker, Abdol Aziz Ould Ismail, Ronald Wolf, Steven Brem, Simon Alexander, Wes Hodges, Ofer Pasternak, **Emmanuel Caruyer**, and Ragini Verma. Freewater estimatoR using iNtErpolated iniTialization (FERNET): Characterizing peritumoral edema using clinically feasible diffusion MRI data. *PLoS ONE*, 15(5):e0233645, May 2020. DOI: 10.1371/journal.pone.0233645. URL `https://www.hal.inserm.fr/inserm-02884608`.

Ofer Pasternak, Nir Sochen, Yaniv Gur, Nathan Intrator, and Yaniv Assaf. Free water elimination and mapping from diffusion mri. *Magnetic Resonance in Medicine: An Official Journal of the International Society for Magnetic Resonance in Medicine*, 62(3):717–730, 2009.

C Pierpaoli and DK Jones. Removing csf contamination in brain dt-mris by using a two-compartment tensor model. In *International Society for Magnetic Resonance in Medicine Meeting*, page 1215, 2004.

Sonia Pujol, William Wells, Carlo Pierpaoli, Caroline Brun, James Gee, Guang Cheng, Baba Vemuri, Olivier Commowick, Sylvain Prima, Aymeric Stamm, et al. The DTI challenge: toward standardized evaluation of diffusion tensor imaging tractography for neurosurgery. *Journal of Neuroimaging*, 25(6):875–882, 2015.

Jonathan Rafael-Patino, David Romascano, Alonso Ramirez-Manzanares, Erick Jorge Canales-Rodríguez, Gabriel Girard, and Jean-Philippe Thiran. Robust monte-carlo simulations in diffusion-mri: Effect of the substrate complexity and parameter choice on the reproducibility of results. *Frontiers in neuroinformatics*, 14:8, 2020.

Jonathan Rafael-Patino, Gabriel Girard, Raphaël Truffet, Marco Pizzolato, **Emmanuel Caruyer**, and Jean-Philippe Thiran. The diffusion-simulated connectivity (DiSCo) dataset. *Data in Brief*, 38: 1–7, October 2021. DOI: 10.1016/j.dib.2021.107429. URL `https://www.hal.inserm.fr/inserm-03366969`.

Gaëtan Rensonnet, Benoît Scherrer, Gabriel Girard, Aleksandar Jankovski, Simon K Warfield, Benoît Macq, Jean-Philippe Thiran, and Maxime Taquet. Towards microstructure fingerprinting: estimation of tissue properties from a dictionary of monte carlo diffusion mri simulations. *NeuroImage*, 184:964–980, 2019.

Gaëtan Rensonnet, Jonathan Rafael-Patiño, Benoît Macq, Jean-Philippe Thiran, Gabriel Girard, and Marco Pizzolato. A signal peak separation index for axisymmetric b-tensor encoding. In *Computational Diffusion MRI*, pages 29–42. Springer, 2021.

Alexis Reymbaut, Alex Valcourt Caron, Guillaume Gilbert, Filip Szczepankiewicz, Markus Nilsson, Simon K Warfield, Maxime Descoteaux, and Benoit Scherrer. Magic diamond: Multi-fascicle diffusion compartment imaging with tensor distribution modeling and tensor-valued diffusion encoding. *Medical Image Analysis*, 70: 101988, 2021.

Francois Rheault, Alessandro De Benedictis, Alessandro Daducci, Chiara Maffei, Chantal MW Tax, David Romascano, Eduardo Caverzasi, Felix C Morency, Francesco Corrivetti, Franco Pestilli, et al. Tractostorm: The what, why, and how of tractography dissection reproducibility. *Human brain mapping*, 41(7):1859–1874, 2020.

L Ruthotto, H Kugel, J Olesch, B Fischer, J Modersitzki, M Burger, and CH Wolters. Diffeomorphic susceptibility artifact correction of

diffusion-weighted magnetic resonance images. *Physics in Medicine & Biology*, 57(18):5715, 2012.

Benoit Scherrer and Simon K Warfield. Why multiple b-values are required for multi-tensor models. evaluation with a constrained log-euclidean model. In *2010 IEEE International Symposium on Biomedical Imaging: From Nano to Macro*, pages 1389–1392. IEEE, 2010.

Benoit Scherrer, Armin Schwartzman, Maxime Taquet, Mustafa Sahin, Sanjay P Prabhu, and Simon K Warfield. Characterizing brain tissue by assessment of the distribution of anisotropic microstructural environments in diffusion-compartment imaging (diamond). *Magnetic resonance in medicine*, 76(3):963–977, 2016.

Kurt G Schilling, François Rheault, Laurent Petit, Colin B Hansen, Vishwesh Nath, Fang-Cheng Yeh, Gabriel Girard, Muhamed Barakovic, Jonathan Rafael-Patino, Thomas Yu, et al. Tractography dissection variability: What happens when 42 groups dissect 14 white matter bundles on the same dataset? *NeuroImage*, 243: 118502, 2021.

Kurt G Schilling, Chantal MW Tax, Francois Rheault, Bennett A Landman, Adam W Anderson, Maxime Descoteaux, and Laurent Petit. Prevalence of white matter pathways coming into a single white matter voxel orientation: The bottleneck issue in tractography. *Human brain mapping*, 43(4):1196–1213, 2022.

Evan Schwab, H Ertan Çetingül, Bijan Afsari, Michael A Yassa, and René Vidal. Rotation invariant features for hardi. In *International Conference on Information Processing in Medical Imaging*, pages 705–717. Springer, 2013.

Robert E Smith, Jacques-Donald Tournier, Fernando Calamante, and Alan Connelly. Sift: Spherical-deconvolution informed filtering of tractograms. *Neuroimage*, 67:298–312, 2013.

Haykel Snoussi, **Emmanuel Caruyer**, Julien Cohen-Adad, Olivier Commowick, Benoit Combes, Elise Bannier, Anne Kerbrat, and Christian Barillot. Geometric evaluation of distortion correction methods in diffusion MRI of the spinal cord. In *ISBI 2019 - 16th IEEE International Symposium on Biomedical Imaging*, pages 1696–1699, Venice, Italy, April 2019. IEEE. DOI: 10.1109/ISBI.2019.8759196. URL `https://www.hal.inserm.fr/inserm-01986723`.

Haykel Snoussi, Julien Cohen-Adad, Olivier Commowick, Benoit Combes, Elise Bannier, Soizic Leguy, Anne Kerbrat, Christian Barillot, and Emmanuel Caruyer. Evaluation of distortion correction methods in diffusion mri of the spinal cord. *arXiv preprint arXiv:2108.03817*, 2021.

Haykel Snoussi, Benoit Combes, Olivier Commowick, Elise Bannier, Anne Kerbrat, Julien Cohen-Adad, Christian Barillot, and

Emmanuel Caruyer. Reproducibility and evolution of diffusion MRI measurements within the cervical spinal cord in multiple sclerosis. In *ISBI 2022 - IEEE International Symposium on Biomedical Imaging*, pages 1–5, Kolkata, India, March 2022. IEEE. URL https://www.hal.inserm.fr/inserm-03639907.

Stamatios N Sotiropoulos, Saad Jbabdi, Junqian Xu, Jesper L Andersson, Steen Moeller, Edward J Auerbach, Matthew F Glasser, Moises Hernandez, Guillermo Sapiro, Mark Jenkinson, et al. Advances in diffusion mri acquisition and processing in the human connectome project. *Neuroimage*, 80:125–143, 2013.

Cibu Thomas, Frank Q Ye, M Okan Irfanoglu, Pooja Modi, Kadharbatcha S Saleem, David A Leopold, and Carlo Pierpaoli. Anatomical accuracy of brain connections derived from diffusion mri tractography is inherently limited. *Proceedings of the National Academy of Sciences*, 111(46):16574–16579, 2014.

Daniel Topgaard. Multidimensional diffusion mri. *Journal of Magnetic Resonance*, 275:98–113, 2017.

Raphaël Truffet, Christian Barillot, and **Emmanuel Caruyer**. Optimal selection of diffusion-weighting gradient waveforms using compressed sensing and dictionary learning. In *ISMRM 2019 - 27th Annual Meeting & Exhibition*, pages 1–3, Montréal, Canada, May 2019. URL https://www.hal.inserm.fr/inserm-02015394.

Raphaël Truffet, Jonathan Rafael-Patino, Gabriel Girard, Marco Pizzolato, Christian Barillot, Jean-Philippe Thiran, and **Emmanuel Caruyer**. An evolutionary framework for microstructure-sensitive generalized diffusion gradient waveforms. In *MICCAI 2020 - 23rd International Conference on Medical Image Computing and Computer Assisted Intervention*, pages 1–11, Lima, Peru, October 2020. URL https://www.hal.inserm.fr/inserm-02910086.

Henning U Voss, Richard Watts, Aziz M Uluğ, and Doug Ballon. Fiber tracking in the cervical spine and inferior brain regions with reversed gradient diffusion tensor imaging. *Magnetic resonance imaging*, 24(3):231–239, 2006.

Van J Wedeen, Patric Hagmann, Wen-Yih Isaac Tseng, Timothy G Reese, and Robert M Weisskoff. Mapping complex tissue architecture with diffusion spectrum magnetic resonance imaging. *Magnetic resonance in medicine*, 54(6):1377–1386, 2005.

C-F Westin, Stephan E Maier, Hatsuho Mamata, Arya Nabavi, Ferenc A Jolesz, and Ron Kikinis. Processing and visualization for diffusion tensor mri. *Medical image analysis*, 6(2):93–108, 2002.

Carl-Fredrik Westin, Hans Knutsson, Ofer Pasternak, Filip Szczepankiewicz, Evren Özarslan, Danielle van Westen, Cecilia Mattisson, Mats Bogren, Lauren J O'Donnell, Marek Kubicki, et al. Q-space trajectory imaging for multidimensional diffusion mri of the human brain. *Neuroimage*, 135:345–362, 2016.

Ilyess Zemmoura, Barthélémy Serres, Frédéric Andersson, Laurent Barantin, Clovis Tauber, Isabelle Filipiak, Jean-Philippe Cottier, Gilles Venturini, and Christophe Destrieux. Fibrascan: a novel method for 3d white matter tract reconstruction in mr space from cadaveric dissection. *Neuroimage*, 103:106–118, 2014.

Hui Zhang, Torben Schneider, Claudia A Wheeler-Kingshott, and Daniel C Alexander. Noddi: practical in vivo neurite orientation dispersion and density imaging of the human brain. *Neuroimage*, 61(4):1000–1016, 2012.